Heliyon 10 (2024) e27022

Contents lists available at ScienceDirect

Heliyon

journal homepage: www.cell.com/heliyon

Research article

Identification of the novel biomarkers involved in the mitochondrial metabolism-related reactive oxygen species and their role in lung cancer T-cell exhaustion and immunotherapy

Sheng Wang [a], Bo Liu [a], Fang Li [a], Zhe Tang [b,***], Xuyu Gu [c,**], Xianglin Yuan [a,*]

[a] Department of Oncology, Tongji Hospital, Tongji Medical College, Huazhong University of Science and Technology, Wuhan, 430030, Hubei, China
[b] Department of Thoracic Surgery, Tongji Hospital, Tongji Medical College, Huazhong University of Science and Technology, Wuhan, 430030, Hubei, China
[c] Department of Oncology, Shanghai Pulmonary Hospital, Tongji University, Shanghai, 200433, China

ARTICLE INFO

Keywords:
Non-small cell lung cancer
Immunotherapy
T lymphocyte failure
Mitochondrial metabolism
ADH1C

ABSTRACT

Purpose: To study the role of mitochondrial metabolism and obtain novel biomarkers in immunotherapy for non-small cell lung cancer (NSCLC).

Methods: We collected the 188 genes involved in mitochondrial metabolism(MMGs) from the MSIGDB project and then quantified the activity of mitochondrial metabolism. All the NSCLC patients were divided into C1 and C2 clusters based on the 26 prognosis-related MMGs. The differences in biology, differential immune microenvironment, chronic hypoxia and prognosis between C1 and C2 patients were also analyzed. In addition, we validated the results of bioinformatics analysis in lung cancer tissues and cell lines.

Results: Patients in the C2 cluster had a higher level of mitochondrial metabolism. Patients in the C2 cluster responded better to immunotherapy and had a lower level of T-cell exclusion. The markers of T-cell failure were upregulated in the C1 patients. Hypoxia can lead to a high percentage of C1 patients. ADH1C might be involved in mitochondrial metabolism and immunotherapy response, which can be affected by hypoxia, making it an underlying biomarker. The expression levels of ADH1C in BEAS-2B, H1299, A549 and H460 cells were detected, revealing that ADH1C is upregulated in lung cancer cells. We observed that patients with low ADH1C expression had a longer survival time. The enzyme activities of HK, PK, LDH and SDH were significantly reduced in H1299 and H460 cells with ADH1C knockdown, along with more ROS. Furthermore, the expression levels of PD-L1 and HHLA2 in tumor tissues were analyzed, which found that ADH1C was significantly positively correlated with the expression of PD-L1 and HHLA2.

Conclusions: In summary, our study comprehensively explored the molecules involved in mitochondrial metabolism and their role in immunotherapy and T lymphocyte failure.

* Corresponding author.
** Corresponding author.
*** Corresponding author.
E-mail addresses: ztang@tjh.tjmu.edu.cn (Z. Tang), guxuyu@126.com (X. Gu), yuanxianglin@hust.edu.cn (X. Yuan).

https://doi.org/10.1016/j.heliyon.2024.e27022
Received 11 November 2023; Received in revised form 22 January 2024; Accepted 22 February 2024
Available online 29 February 2024

1. Introduction

Lung cancer has been a leading threat to public health globally, with an estimated 2.5 million new cases per year currently [1]. Among all cases, non-small cell lung cancer (NSCLC) is the most common pathological subtype. Clinically, surgical treatment of early-stage lung cancer can often lead to long-term survival [2–4]. Nonetheless, for those in the advanced stage, the therapy options are often limited. Recently, immunotherapy has shown promising performance in lung cancer, especially for specific populations [5].

The environment surrounding tumors is extremely complex, consisting of multiple types of cells and interactions, also called the tumor microenvironment (TME). Meanwhile, the specific component in the TME can be a therapeutic target [6,7]. In the TME, T lymphocyte failure occurs widely after continuous antigen stimulation, hypoxia and nutritional stress [8]. T lymphocyte failure significantly affects epigenetic remodelling and metabolic reprogramming. Intense mitochondrial remodelling, including morphological and kinetic changes, occurs during T-cell activation and effector and memory differentiation [9]. Research has usually observed damaged or broken mitochondria in tumor-infiltrated T lymphocytes [10]. In lung cancer, a study revealed that tissue-resident memory T cells are highly infiltrated when M1 hot tumor-associated macrophages are present in the lung cancer TME [11]. Meanwhile, reactive oxygen species (ROS) are critical for activated T cells to obtain effective functions. Impaired mitochondrial metabolic abnormalities are often associated with T lymphocyte failure due to abnormal mitochondrial ROS and oxidative phosphorylation [12]. Moreover, T lymphocyte failure is involved in cancer immunotherapy. For instance, Yu et al. found that T-cell elimination mediated by macrophages can significantly affect immunotherapy efficacy in liver cancer [13]. Furthermore, oxidative stress and mitochondrial autophagy in tumor cells can be mediated by chronic hypoxia exposure [14]. Consequently, exploring the underlying interaction of mitochondrial metabolism and T lymphocyte failure in lung cancer is meaningful.

In this study, we collected 188 MMGs (mitochondrial metabolism genes) from the MSIGDB project and quantified the activity of mitochondrial metabolism. All NSCLC patients were divided into C1 and C2 clusters based on the 26 prognosis-related MMGs. The results indicated that the patients in the C2 cluster had a higher level of mitochondrial metabolism. The correlation analysis showed that the C2 patients had a higher percentage of older patients, indicating different metabolism patterns in patients of different ages. Evidence from the TCGA and combined GEO cohorts indicated that patients in the C2 cluster responded better to immunotherapy and had a lower level of T-cell exclusion. Moreover, we found that all the markers of T-cell failure were upregulated in the C1 patients. The biological and immune microenvironment differences were then investigated between C1 and C2 patients. Notably, we found that hypoxia can lead to a high percentage of C1 patients. Through further exploration of prognosis-related MMGs, we found that ADH1C might be involved in mitochondrial metabolism and immunotherapy response, which can be affected by hypoxia, making it an underlying biomarker.

2. Methods

2.1. Data collection

Data on the expression profile and clinical features of lung cancer patients were collected from The Cancer Genome Atlas (TCGA) and Gene Expression Omnibus (GEO) databases. The form of the expression profile was “STAR-Counts”, which was collated using R and Perl code. For the GEO database, the GSE30219, GSE37745 and GSE50081 cohorts were identified, whose platform was GPL570. The list of mitochondrial metabolism genes (MMGs) was obtained from the https://www.gsea-msigdb.org/website and is shown in Table S1. The data preprocessing process was conducted before analysis. Data combination of the GEO cohort was performed using the sva package.

2.2. Genotyping

Univariate Cox regression was utilized to identify MMGs related to patient prognosis. Based on the above prognosis-related MMGs, genotyping was conducted using the ConsensusClusterPlus package.

2.3. Enrichment score

The gene set variation analysis package (GSVA) and its extended function ssGSEA were utilized to quantify the enrichment score based on specific genes [15]. The reference genes or gene sets included the hallmark gene set and 188 MMGs.

2.4. Biological enrichment

GSEA was performed to investigate the underlying biological differences between the two groups [16]. The reference set was Hallmark. Visualization was performed using the fgsea package.

2.5. Protein–protein interaction (PPI) network

The interaction of specific proteins was investigated using the STRING database (https://cn.string-db.org/). Specifically, the interaction score was set to 0.4. The meaning of network edges was set as “evidence”. Cytoscape software was used for visualization.

2.6. Evaluation of immunotherapy response

The assessment of the immunotherapy response of lung cancer patients was administered with the Tumor Immune Dysfunction and Exclusion (TIDE) algorithm [17]. Patients with TIDE <0 were defined as immunotherapy responders; otherwise, they were defined as nonresponders.

2.7. Immune cell quantification

Quantification of the immune microenvironment was conducted using the CIBERSORT algorithm [18]. The CIBERSORT algorithm can quantify the relative infiltration levels of 22 kinds of immune cells based on the input gene expression profile.

2.8. Quantitative real-time (qRT) PCR

Total RNA was extracted by adding TRIzol (containing DNaseI) to the tissue or cultured cells according to the manufacturer's protocol (Invitrogen, China). cDNA was generated through reverse transcription based on a commercial cDNA synthesis kit (Thermo-Fisher, China). The SYBR Green Master Mix system (Invitrogen, China) was utilized for qRT−PCR. The mRNA level of GAPDH was chosen as an internal control gene for normalization. The gene expression level of specific genes was quantified using the $2^{-\Delta Ct}$ method.

2.9. Immunohistochemistry (IHC)

Five-micron-thick sections of tumor tissues were cut and embedded. IHC was performed through the SP method using the AHD1C primary antibody (#PA5-76340, Thermo Fisher). Positive expression was observed as yellow, brown or tan cytoplasmic staining. The AHD1C index was calculated based on the percentage of positive cells in 10 randomly selected fields of view.

2.10. Cell culture

H1299 (#1101HUM-PUMC000469, CCRID), BEAS-2B (#3101HUMSCSP5067, CCRID), H1460 (#1101HUM-PUMC000355, CCRID) and A549 (#1101HUM- PUMC000002, CCRID) cells were purchased from Cell Resource Center of Peking Union Medical College (PCRC, Beijing, China) and cultured using the RPMI-1640 with 10% fetal bovine serum. The medium was added with the double antibody of 100U/ml penicillin and 100 mg/ml streptomycin.

2.11. Western blot

The radioimmunoprecipitation method was utilized to extract the protein, and 1% benzylsulfonyl fluoride and 1% phosphate inhibitor were added. The SDS−PAGE gel was used for the Western blot. The antibodies used were GAPDH (ab8275, Abcam) and ADH1C (#PA5-76340, Thermo Fisher).

2.12. TEM

H1299 and H460 cells were collected and then fixed with 2.5% paraformaldehyde and 1.5% osmic acid solution. Next, the cells were dehydrated with ethanol of gradient concentrations, embedded in paraffin, sliced at 70 nm and stained with uranyl acetate and lead citrate. Autophagosome and autolysosome were observed under the TEM (JEM).

2.13. Mitotracker

Reactive oxygen species (ROS) formation in THP1 macrophages was determined using the MitSOX™ red mitochondrial superoxide indicator (Invitrogen, Waltham, USA) according to the manufacturer's instructions. H1299 and H460 cells were grown on cover slips and treated with a 5 μM MitoSOX reagent working solution for 10 min at 37 °C. Subsequently, coverslips were washed three times with warm 1× PBS and imaged using a fluorescence microscope (Keyence, Osaka, Japan).

2.14. TUNEL

The cell suspension was seeded into confocal culture dishes and placed in 50 mL/L CO2 cell incubators at 37 °C for routine culture. When the cell confluence was above 80%, the TUNEL staining was performed according to the instructions of TUNEL kit (R&D system, Minneapolis, MN, USA). Finally, the nuclei were stained with 10 μg/mL 4′,6-diamidino-2-phenylindole (DAPI; Wuhan Google Biotech Co., Ltd., Wuhan, China) for 10 min. The apoptotic cells were observed under a confocal microscope (Olympus) to calculate the TUNEL-positive rate.

2.15. ELISA

The supernatant of 0.5 mL medium was taken, centrifuged at 3500 r/min for 10 min, and then frozen for ELISA detection. The ELISA kit was left at room temperature for 30 min, and the standard substance was diluted according to the needed concentration. Serum (100 μL) and standard substance were added to each well and treated at 36 °C for 90 min. After washing the plate, 100 μL of biotinized antibody was added to each reaction well, and antibody diluent was added to the blank well for 60 min. After washing the plate, 100 μL of enzyme-labelled antibody was added to each reaction well, and the dilutive solution of enzyme binding was added to the blank well for 30 min. After washing the plate, 100 μL of 3,3′,5,5′-tetramethylbenzidine (TMB) was added to each well for color development for 15 min. Then, 100 μL termination solution was added, the absorbance (A value) of each specimen was read by enzyme marker within 3 min, and the standard curve was drawn according to the concentration of standard substance and corresponding A value.

2.16. Statistical analysis

All analyses were performed using R code and GraphPad Prism 8. Comparisons with a P value < 0.05 were considered statistically significant. According to the distribution of data, Student's *t*-test and the Mann–Whitney *U* test were used. Differentially expressed

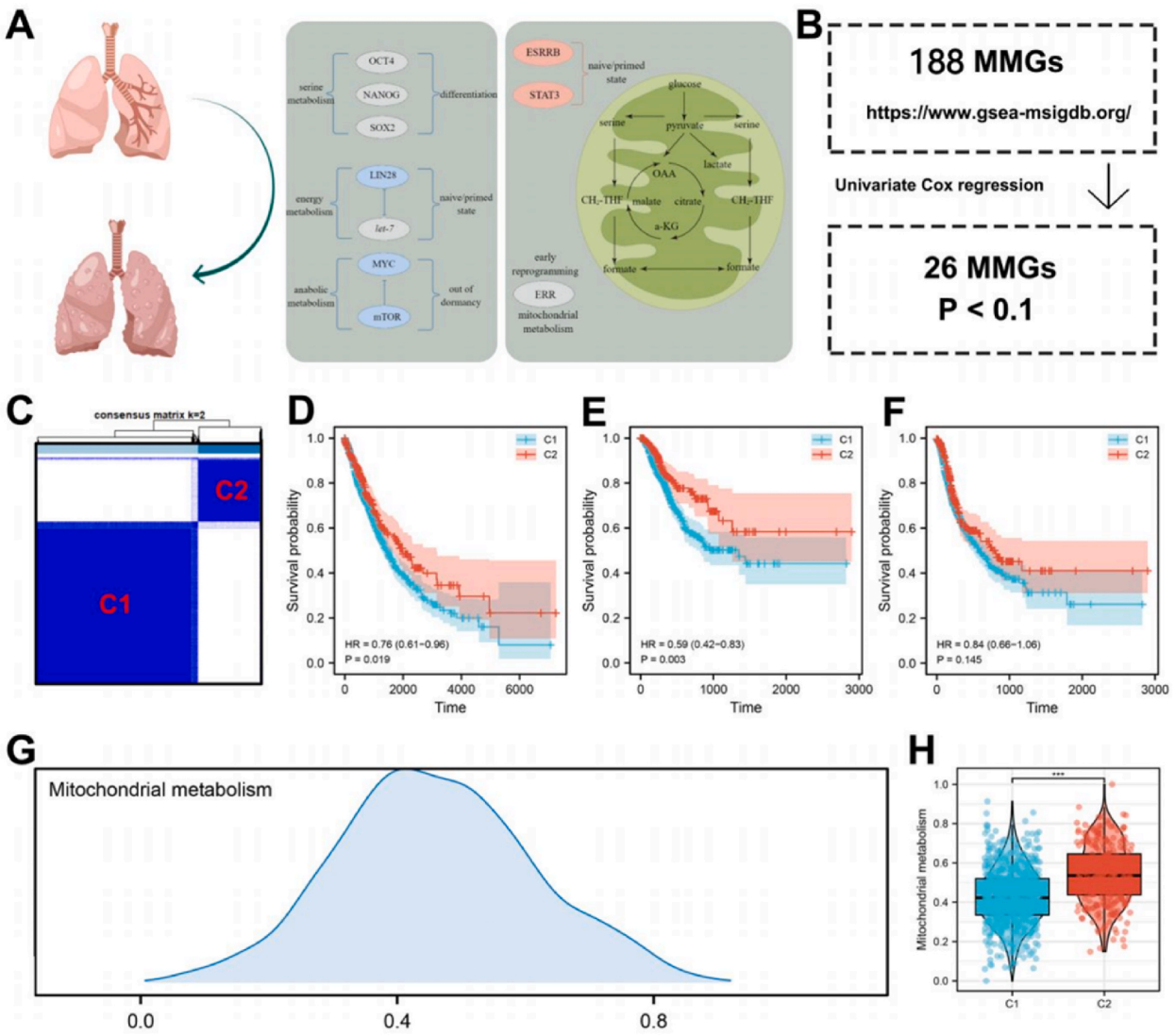

Fig. 1. Data collection and quantification of mitochondrial metabolism. **Notes: A:** Lung cancer is accompanied by extensive mitochondrial metabolic abnormalities; **B:** MMGs obtained from the MSIGDB project; **C:** Genotyping based on the prognosis-related MMGs; **D-F:** Overall survival, disease-free survival and progression-free survival of C1 and C2 patients; **G:** The quantified level of mitochondrial metabolism; **H:** The level of mitochondrial metabolism on C1 and C2 patients.

gene (DEG) analysis was performed using the limma package with a specific threshold.

3. Results

3.1. Genotyping based on the collected MMGs

Generally, lung cancer is accompanied by extensive mitochondrial metabolic abnormalities (Fig. 1A). Therefore, we tried to explore mitochondrial metabolism in lung cancer. A total of 188 MMGs were collected from the MSIGDB project (Fig. 1*B, Supplementary file 1*). Then, a univariate Cox regression analysis was conducted to identify prognosis-related MMGs, which are shown in ***Table 1***. All NSCLC patients were divided into C1 and C2 clusters based on the 26 prognosis-related MMGs (Fig. 1C). Kaplan–Meier survival curves indicated that the patients in C1 might have worse survival than those in the C1 cluster, including overall survival and disease-free survival (***Fig. 1D–E***). Meanwhile, although the statistical P value of progression-free survival was not significant (P = 0.145), a clear distinction can also be observed in the survival curve between C1 and C2 (Fig. 1F). Based on the collected MMGs, the enrichment score of mitochondrial metabolism was determined (Fig. 1G). The results indicated that the patients in the C2 cluster had higher mitochondrial metabolism activity (Fig. 1H).

3.2. Clinical differences

Next, we found that most of the prognosis-related MMGs had a different expression pattern between patients in the C1 and C2 clusters (Fig. 2A). We next explored the clinical differences in C1 and C2 patients, including sex, age and clinical stage (Fig. 2B–G). The results showed that only age differences were observed in C1 and C2 patients, and the C2 cluster had a higher percentage of >65-year-old patients (Fig. 2D). Three independent cohorts, GSE30219, GSE37745 and GSE50081, were selected for further analysis, and significant batch effects were observed (Fig. 2E). The Sva package was utilized to reduce batch effects and perform data combination (Fig. 2F).

3.3. Immunotherapy evaluation

Mitochondrial metabolism can affect the status of T lymphocytes, which might have an underlying influence on lung cancer immunotherapy. TIDE analysis was utilized to calculate the TIDE score and the status of T lymphocytes in the TCGA and GEO cohorts (Fig. 3A–B). In the TCGA cohort, the results showed that the C1 cluster had a higher TIDE score (Fig. 3C). For T lymphocytes, we found that the patients in the C1 cluster had higher T-cell exclusion but not T-cell dysfunction (Fig. 3D–E). Additionally, 47.4% of patients in the C2 cluster were considered immunotherapy responders, which was significantly 31.5% in the C1 cluster (Fig. 3F). Meanwhile, the same trend was observed in the combined GEO cohort (Fig. 3G–J). Furthermore, we evaluated the markers of T lymphocyte failure in C1 and C2 patients. The results showed that all these markers were overexpressed in C1 patients, including CTLA4, TIGIT, PDCD1 and

Table 1
The prognosis related MMGs.

ID	HR	HR.95L	HR.95H	pvalue
PFKP	1.21	1.09	1.34	0.00
ACSL3	1.28	1.10	1.48	0.00
GAPDH	1.16	1.05	1.29	0.00
ADH4	1.22	1.07	1.39	0.00
ADH1C	0.94	0.90	0.98	0.01
ALDH7A1	1.12	1.03	1.21	0.01
PGM2	1.14	1.04	1.26	0.01
AKR1A1	0.76	0.62	0.94	0.01
GCDH	0.79	0.66	0.95	0.01
PPARD	1.22	1.04	1.43	0.01
ACADSB	0.87	0.77	0.98	0.02
OGDH	1.22	1.02	1.47	0.03
ACSL4	1.13	1.01	1.26	0.03
CYP2U1	0.87	0.76	0.99	0.03
SDHA	1.17	1.00	1.38	0.06
PPAT	1.13	1.00	1.27	0.06
IDH3B	1.19	0.99	1.42	0.06
NDUFS1	1.20	0.99	1.45	0.06
ACAT2	1.11	0.99	1.23	0.06
NDUFA8	1.18	0.98	1.41	0.07
ATP4B	0.85	0.71	1.02	0.08
PPARG	1.08	0.99	1.17	0.08
NDUFB1	0.85	0.71	1.02	0.08
MDH2	1.17	0.98	1.40	0.08
NDUFA7	0.85	0.70	1.03	0.10
OXCT2	0.86	0.71	1.04	0.10

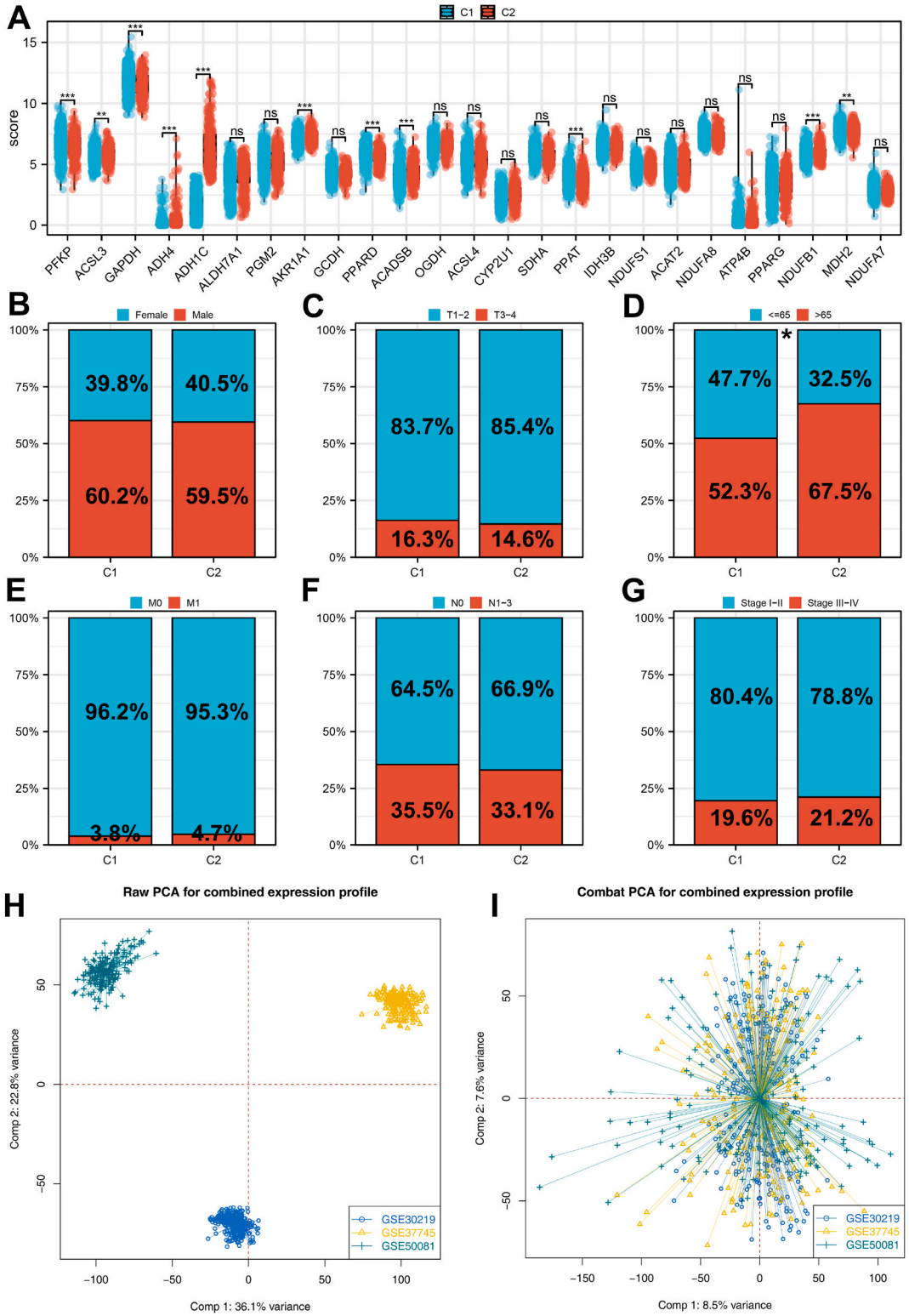

Fig. 2. Clinical correlation and data combination. **Notes: A:** The level of prognosis-related MMGs in C1 and C2 patients; **B-G:** The percentage of clinical features in C1 and C2 patients; **H:** Three independent GEO cohorts were selected; **I:** Sva package was used for data combination.

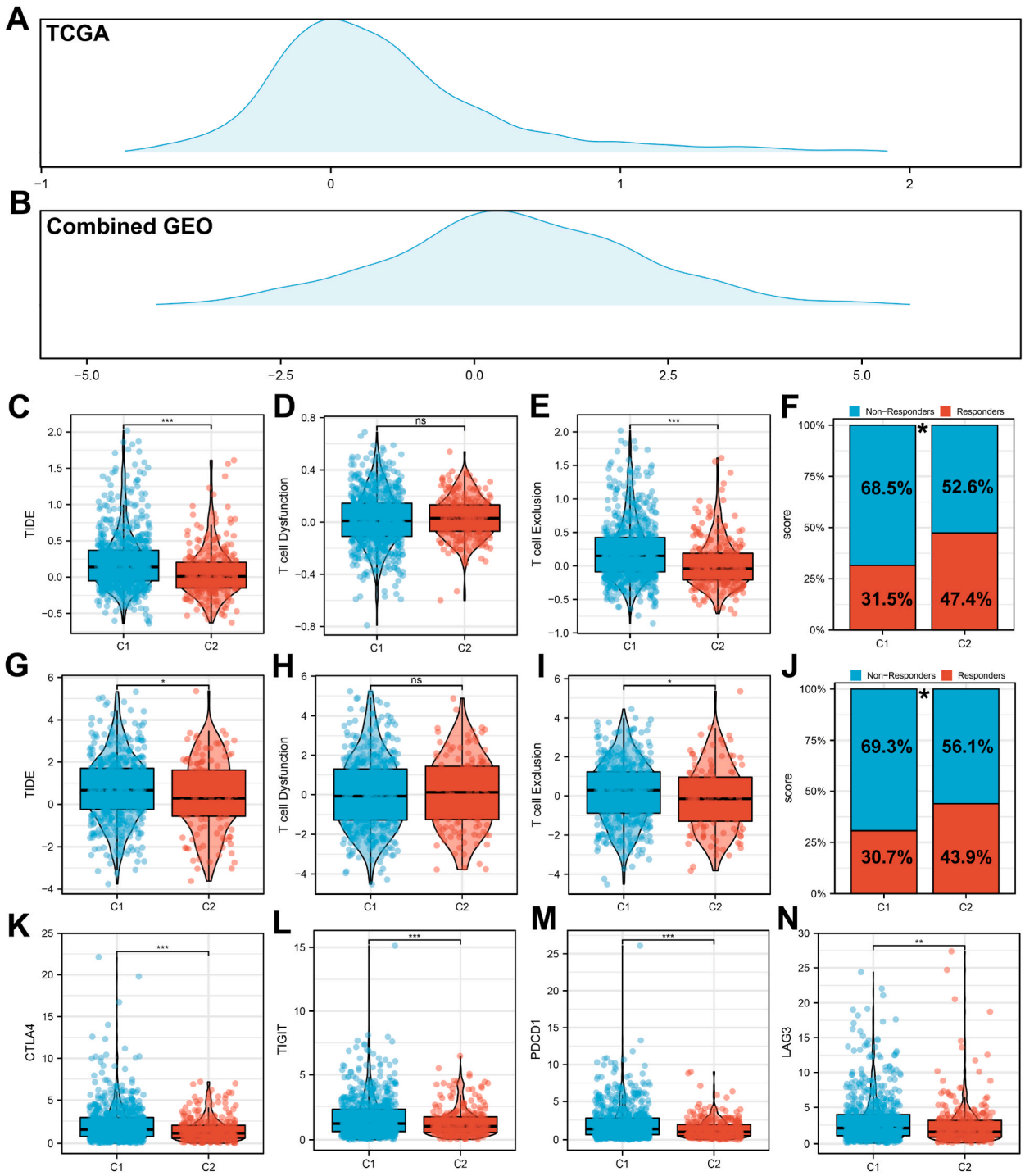

Fig. 3. Immunotherapy evaluation. **Notes: A-B:** The calculated TIDE score in TCGA and combined GEO cohort; **C-E:** The level of TIDE score, T cell dysfunction and T cell exclusion in C1 and C2 patients (TCGA cohort); **F:** The percentage of immunotherapy responders in C1 and C2 patients (TCGA cohort); **G-I:** The level of TIDE score, T cell dysfunction and T cell exclusion in C1 and C2 patients (combined GEO cohort); **J:** The percentage of immunotherapy responders in C1 and C2 patients (combine GEO cohort); **K–N:** The level of CTLA4, TIGIT, PDCD1 and LAG3 in C1 and C2 patients.

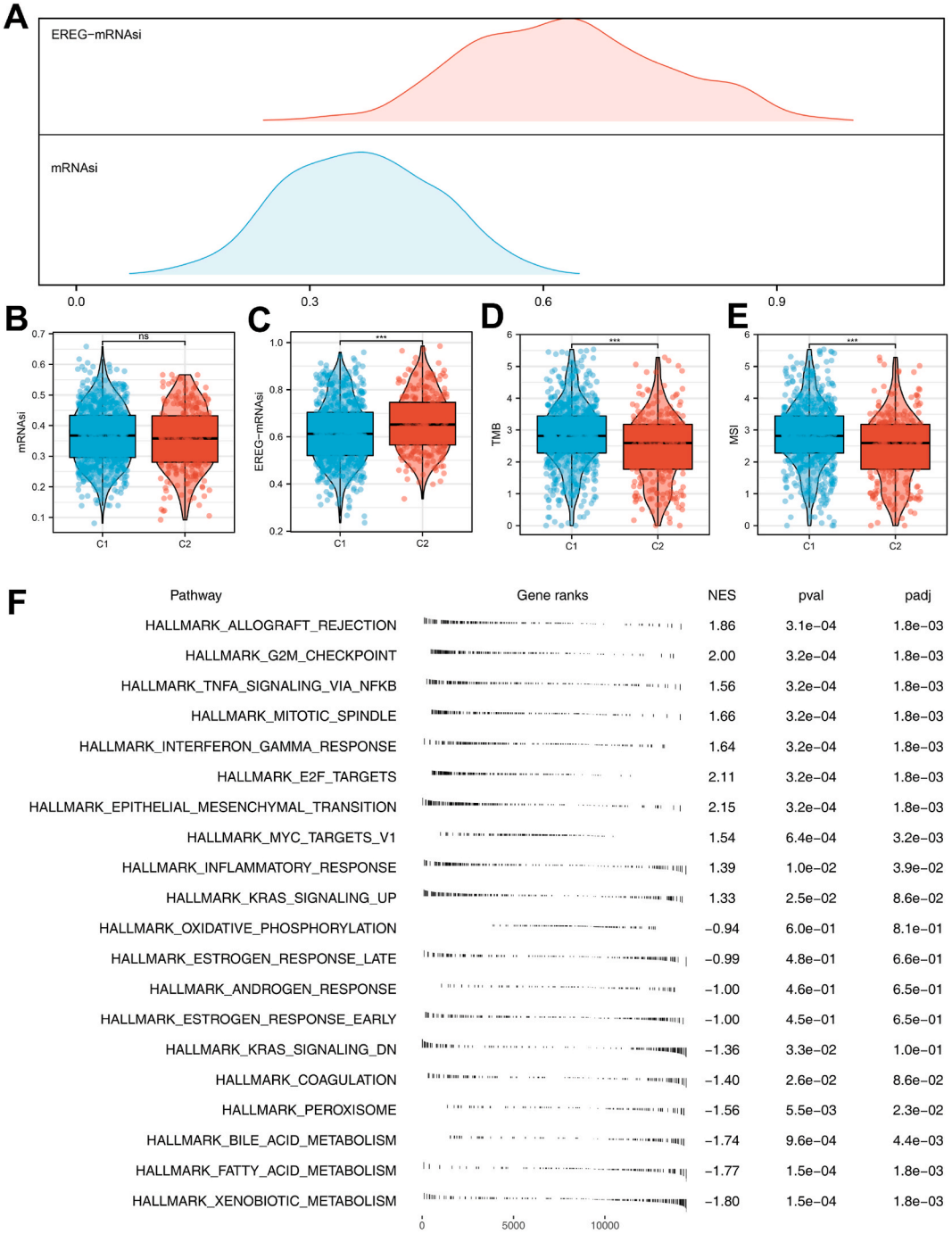

Fig. 4. Biological difference. **Notes: A:** Tumor stemness index of TCGA patients (mRNAsi and EREG-mRNAsi); **B-E:** The level of mRNAsi, EREG-mRNAsi, TMB and MSI in C1 and C2 patients; **F:** GSEA analysis based on Hallmark gene set.

LAG3 (Fig. 3K–N).

3.4. Biological differences between C1 and C2 patients

Tumor stemness can affect the prognosis performance of cancer patients. Based on a previous study, we extracted the tumor stemness index of lung cancer patients in the TCGA database (Fig. 4A). No significant difference was found between C1 and C2 patients in mRNAsi score (Fig. 4B). However, we noticed a higher EREG-mRNAsi level in C2 patients (Fig. 4C). For the TMB and MSI levels, the

patients in the C1 cluster were higher than the patients in the C2 cluster (Fig. 4D–E). GSEA indicated that the terms allograft rejection, G2M checkpoints, TNF-α signaling, mitotic spindle, interferon gamma response, E2F targets, epithelial-mesenchymal transition (EMT), MYC targets, inflammatory response and KRAS signaling were significantly enriched in C1 patients (Fig. 4F).

3.5. Immune microenvironment differences

The CIBERSORT algorithm was utilized to assess the immune microenvironment in lung cancer tissue (Fig. 5A). The results

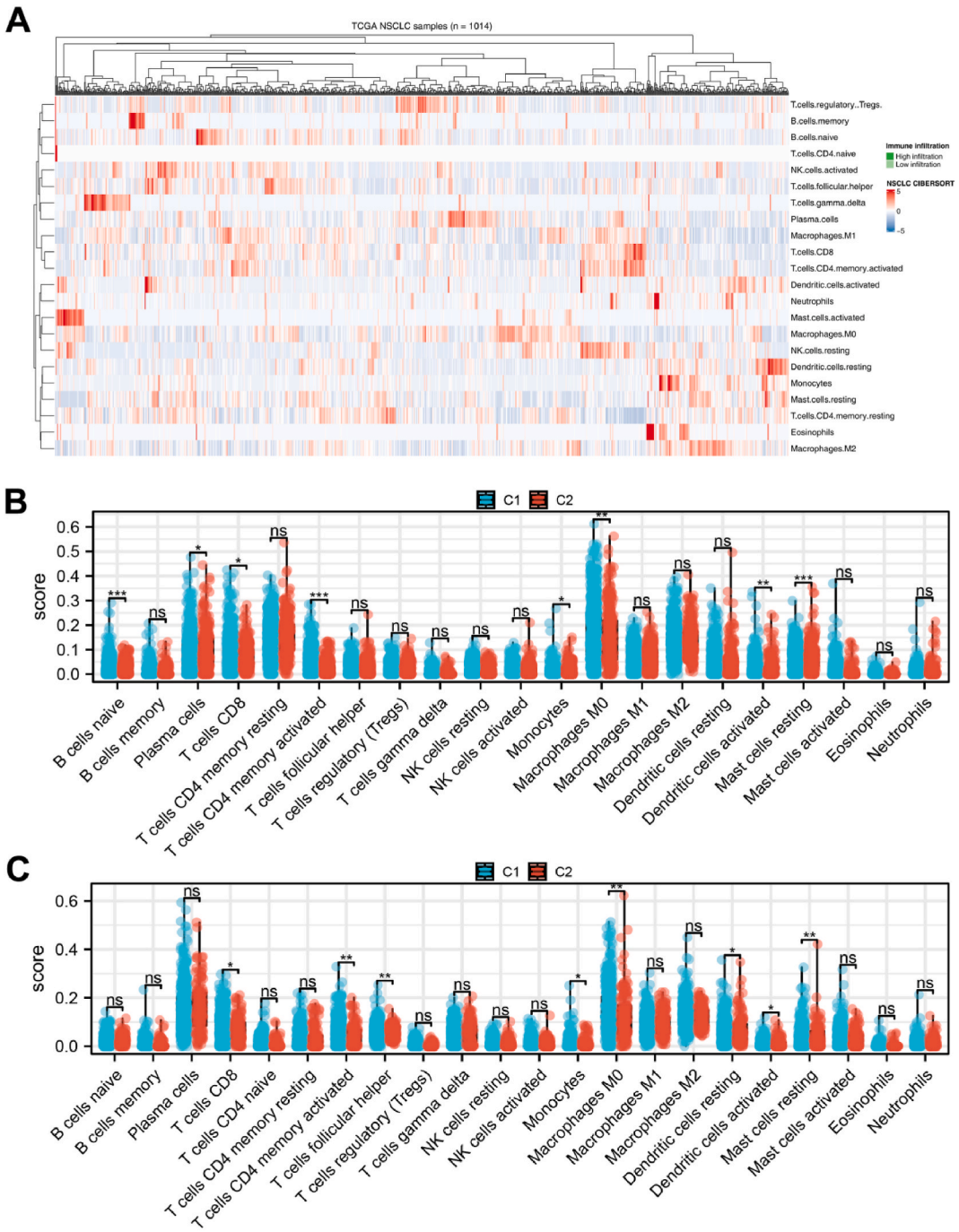

Fig. 5. Immune microenvironment analysis. **Notes: A:** The CIBERSORT algorithm was utilized to quantify the immune microenvironment of lung cancer samples; **B:** The immune microenvironment difference between C1 and C2 patients (TCGA cohort); **C:** The immune microenvironment difference between C1 and C2 patients (combined GEO cohort).

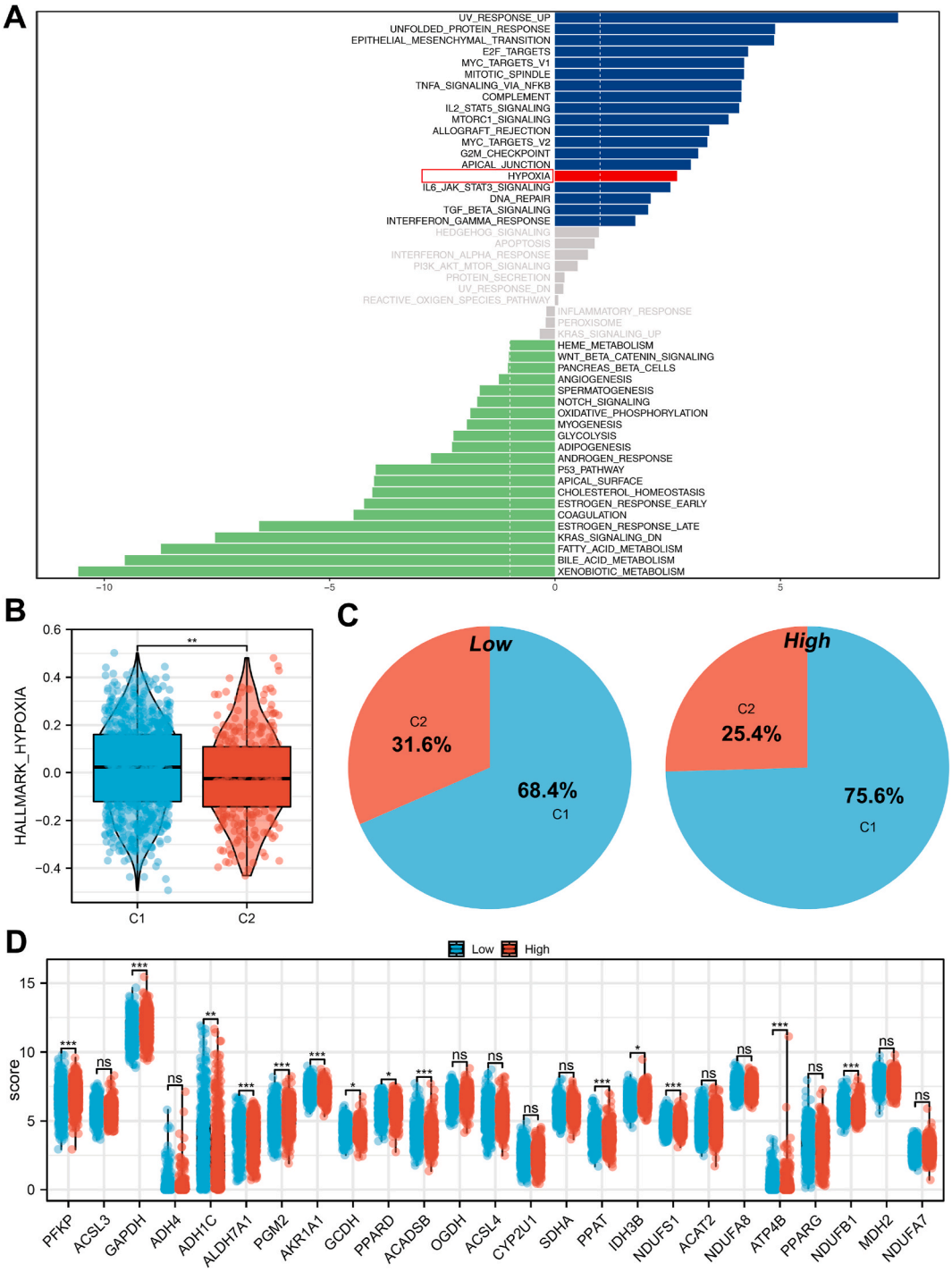

Fig. 6. Hypoxia is associated with a higher percentage of C1 cluster patients. **Notes: A:** GSVA analysis; **B:** The activity of hypoxia in C1 and C2 patients; **C:** The percentage of C1 and C2 patients in patients with high and low hypoxia activity; **D:** The prognosis-related MMGs in patients with high and low hypoxia.

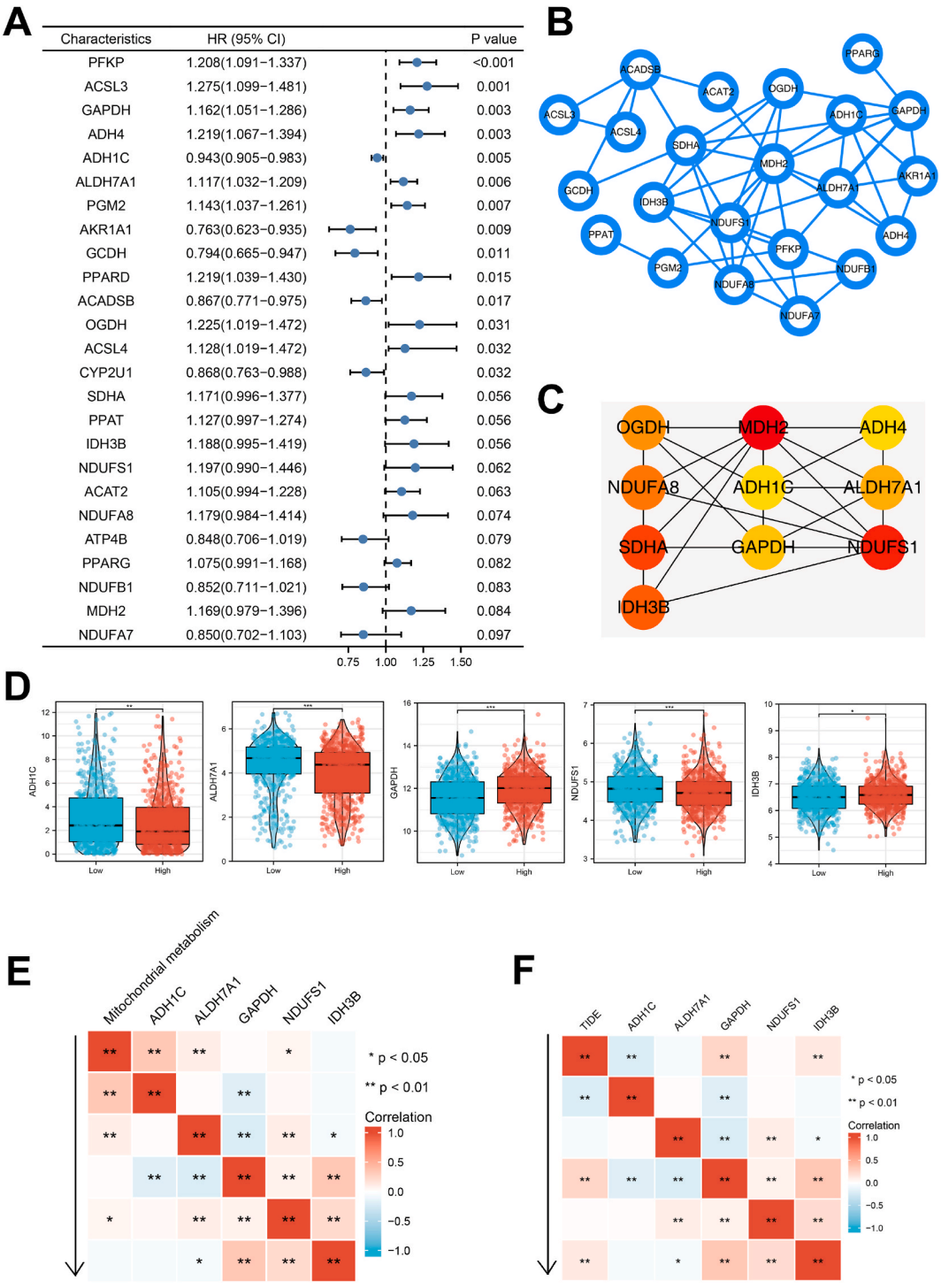

Fig. 7. Further exploration of the prognosis-related MMGs. **Notes: A:** The HR and P value of the prognosis-related MMGs; **B:** PPI network; **C:** Top ten important nodes of the PPI network; **D:** The level of ADH1C, ALDH7A1, GAPDH, NDUFS1 and IDH3B in C1 and C2 patients; **E:** Correlation of ADH1C, ALDH7A1, GAPDH, NDUFS1, IDH3B and mitochondrial metabolism; **F:** Correlation of ADH1C, ALDH7A1, GAPDH, NDUFS1, IDH3B and TIDE.

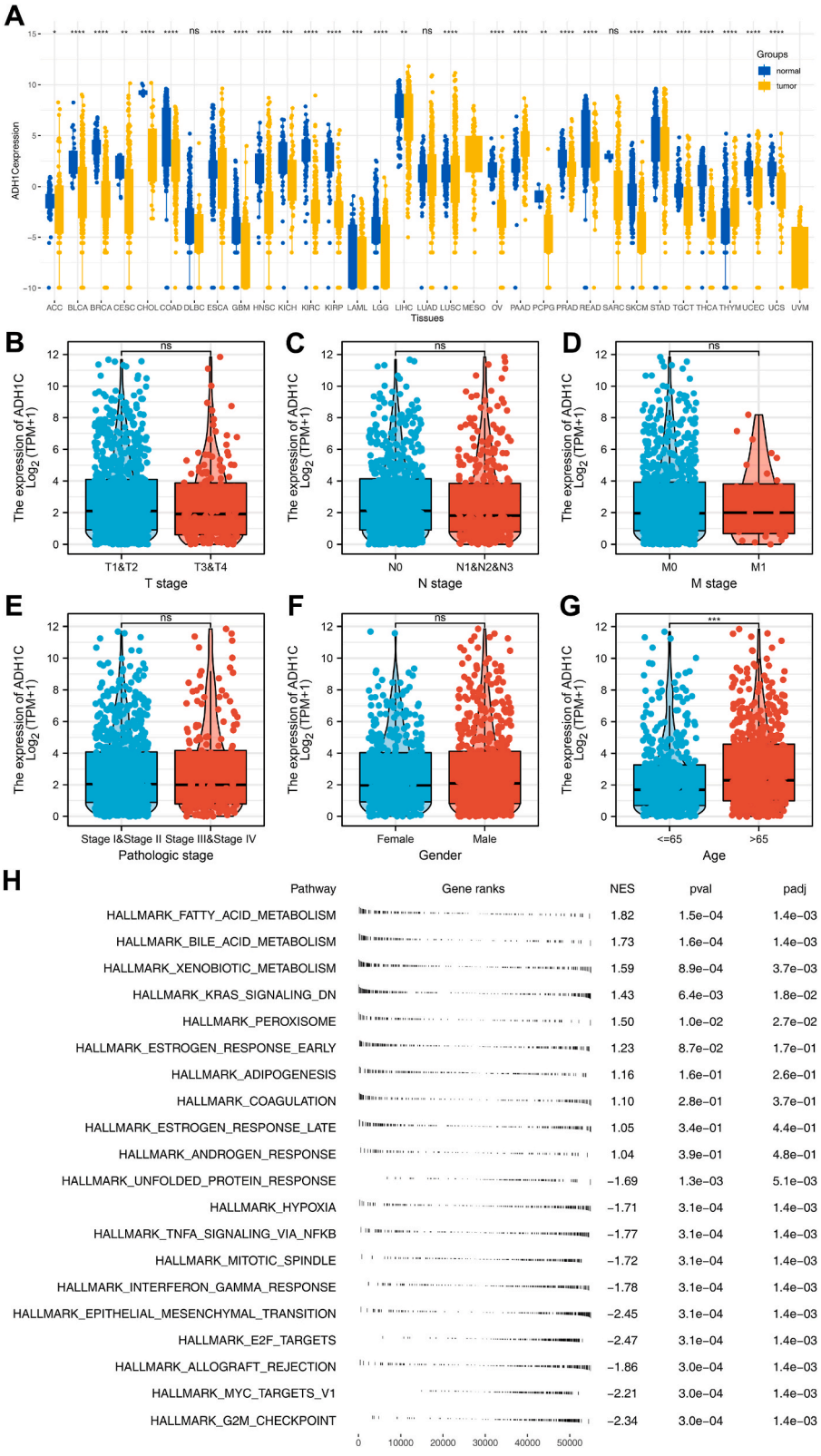

Fig. 8. Role of ADH1C in lung cancer. **Notes: A:** Pan-cancer analysis of ADH1C; **B-G:** Clinical correlation of the ADH1C; **H:** Biological enrichment analysis of ADH1C.

revealed that naive B cells, plasma cells, CD8$^+$ T cells, activated CD4$^+$ memory T cells, M0 macrophages, activated dendritic cells and resting mast cells were upregulated, while monocytes were downregulated in C1 patients in the TCGA cohort (Fig. 5B). In the combined GEO cohort, CD8$^+$ T cells, activated memory CD4$^+$ T cells, follicular helper T cells, monocytes, M0 macrophages, and resting mast cells were upregulated in C1 patients (Fig. 5C).

3.6. *Hypoxia is associated with a higher percentage of C1 cluster patients*

Because chronic hypoxia can induce oxidative stress and mitochondrial dysfunction [10], we performed GSVA analysis in patients with the C1 and C2 clusters. The results showed that hypoxia activity was abnormally activated in C1 patients (Fig. 6A–B). Meanwhile,

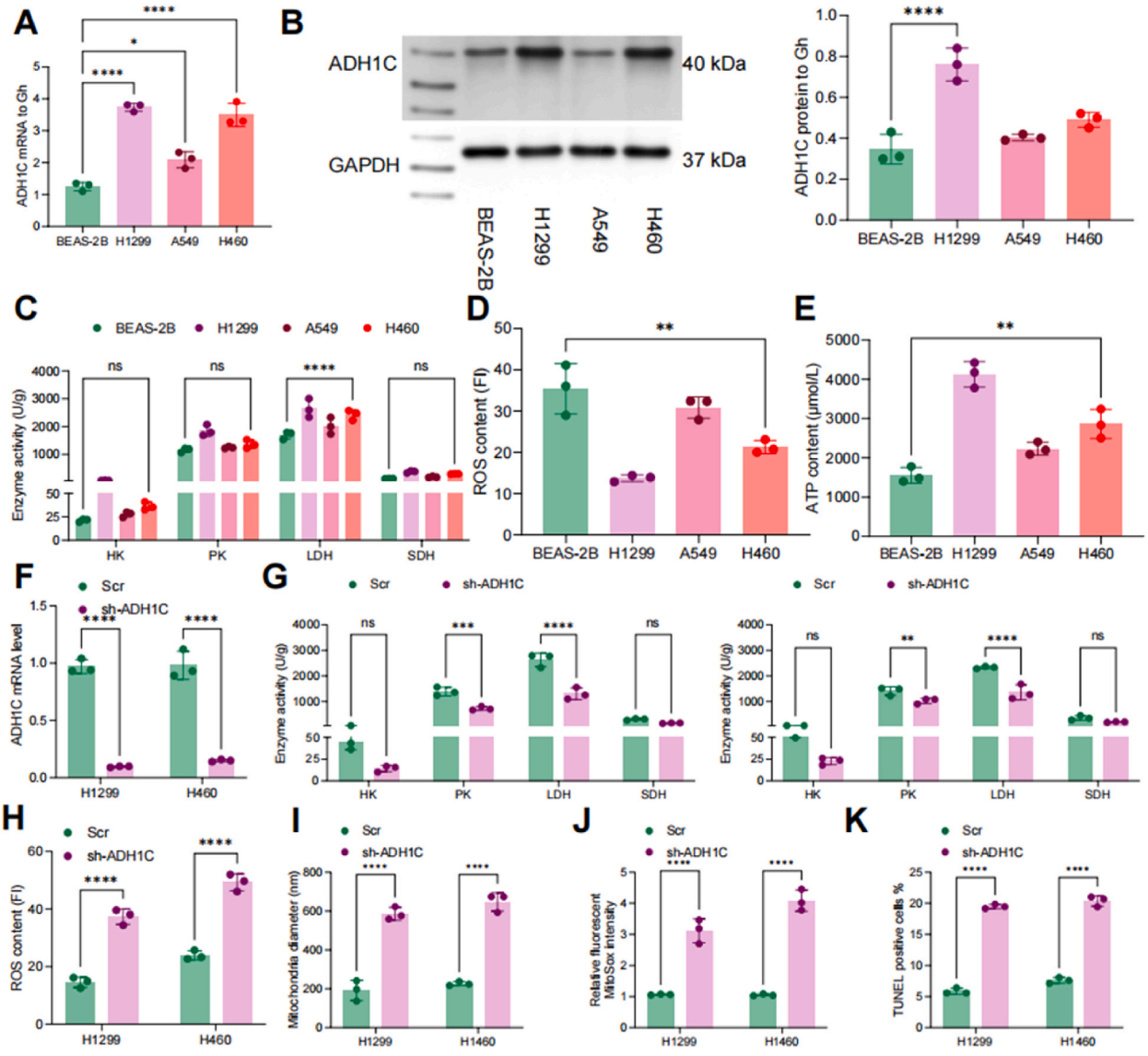

Fig. 9. ADH1C is upregulated in lung cancer cells and associated with ROS

Notes: A: qRT-PCR was utilized to detect the mRNA level of ADH1C in different cell lines; **B:** Western blot was utilized to detect the protein level of ADH1C in different cell lines. **C:** ELISA for HK, PK, LDH and SDH in BEAS-2B and H1299, A549 and H460 cells; **D:** Detection of ROS in BEAS-2B and H1299, A549 and H460 cells; **E:** Bioluminescence assay for ATP in BEAS-2B and H1299, A549 and H460 cells. **F**: qRT-PCR was utilized for ADH1C silencing via sh-ADH1C in H1299 and A549 cells. **G**: ELISA for HK, PK, LDH and SDH in H1299 and A549 cells. **H**: Detection of ROS in H1299 and A549 cells. **I:** TEM detection of mitochondrial diameter in H1299 and H460 cells. **J:** Mitotracker analysis of ROS levels in H1299 and H460 cells. **K**: TUNEL staining to detect the proportion of apoptotic cells in H1299 and H460 cells. Data are presented as mean plus or minus standard deviation using paired *t*-test as well as one-way anova, ANOVA followed by Tukey's multiple comparison test to detect significant differences between data, $^{**}P < 0.01$.

we found that in the patients with high hypoxia activity, the percentage of C1 patients was higher than that in the patients with low hypoxia activity (Fig. 6C, 75.6% vs 68.4%). Furthermore, we detected the expression pattern of prognosis-related MMGs in patients with low and high hypoxia activity (Fig. 6D).

3.7. Further exploration of prognosis-related MMGs

The HR and P value of prognosis-related MMGs are shown in Fig. 7A. The PPI network is shown in Fig. 7B. The cytoHubba plug-in unit of Cytoscape software was used to identify the top ten important nodes (Fig. 7C). Among these, we found that ADH1C, ALDH7A1, and NDUFS1 were overexpressed, while GAPDH and IDH3B were downregulated in patients with low hypoxia activity (Fig. 7D). Correlation analysis indicated that ADH1C, ALDH7A1 and NDUFS1 were positively correlated with mitochondrial metabolism (Fig. 7E); ADH1C was negatively correlated, while GAPDH and IDH3B were positively correlated with the TIDE score (Fig. 7F). We further explored the underlying role of ADH1C. Pancancer analysis was performed to illustrate the expression pattern of ADH1C in multiple cancers (Fig. 8A). Clinical correlation analysis of ADH1C was then performed. The results indicated that ADH1C was highly

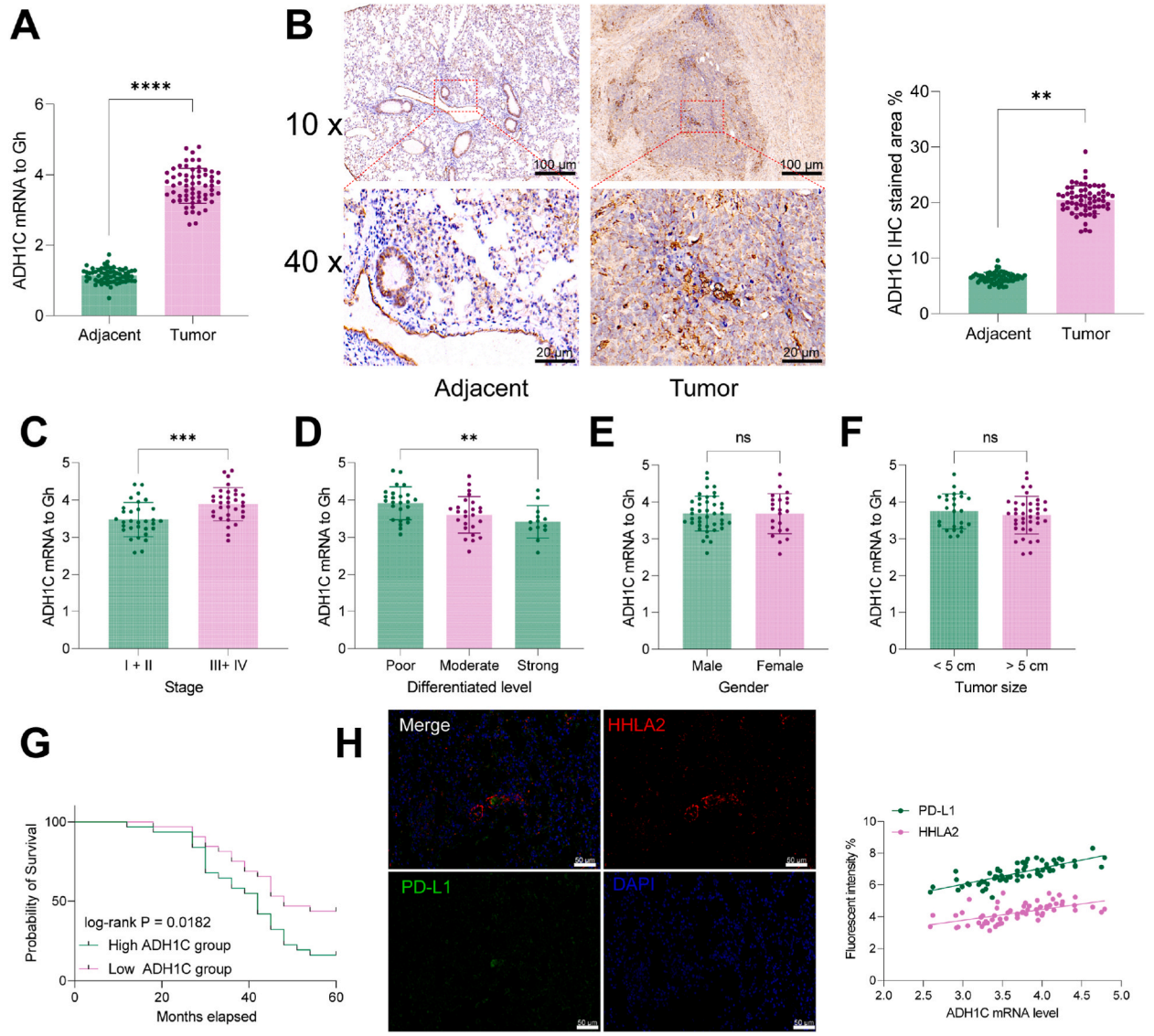

Fig. 10. Correlation analysis of ADH1C and prognosis and immunotherapy in patients with lung cancer. **A:** The mRNA level of ADH1C in three paired lung cancer and control tissue; **B:** Immunohistochemical staining was used to detect the staining intensity of ADH1C in cancer tissues and adjacent tissues; **C–F:** The relationship between the expression level of ADH1C mRNA and clinical TNM stage, tumor differentiation, sex and tumor size in 63 patients with lung cancer was analyzed; **G:** The correlation of ADH1C and the prognosis of 60-month survival of patients were analyzed by Kaplan-Meier analysis; **H:** The expression levels of PD-L1 and HHLA 2 in tumor tissues were determined by immunofluorescence and were also associated with ADH1C by Spearman correlation analysis.

expressed in patients over 65 years old (−). The enrichment analysis indicated that the fatty acid metabolism, bile acid metabolism, xenobiotic metabolism, KRAS signaling, peroxisome, and early estrogen response pathways were significantly enriched in the patients with high ADH1C expression (Fig. 8H).

3.8. ADH1C is upregulated in lung cancer cells and associated with ROS

According to the results of our previous bioinformatics analysis, there is a significant negative correlation between ADH1C and TIDE in lung cancer patients. Moreover, we found that the expression of ADH1C was significantly increased in people over 65 years old. ADH1C was significantly related to the activity of fatty acid metabolism, butyric acid metabolism, KRAS signaling and other pathways. Therefore, we conducted qRT−PCR and WB to verify the expression level of ADH1C in BEAS-2B, H1299, A549 and H460 cells. The results demonstrated that the expression level of ADH1C in BEAS-2B cells was significantly lower than that in lung cancer cell lines, including H1299, A549, and H460 cells (Fig. 9A–B).

Considering that low hypoxia may cause oxidative stress, leading in turn to mitophagy production, we further measured the activities of HK, PK, LDH and SDH, which represent oxidative stress and energy metabolism, in BEAS-2B, H1299, A549 and H460 cells using ELISA. We observed that the activities of HK, PK, LDH and SDH were significantly higher in lung cancer cell lines than in BEAS-2B cells (Fig. 9C), which indicated that energy metabolism was significantly higher in lung cancer cells. Moreover, we further examined the amount of ROS and ATP in the cells, and we observed that the content of ROS in the BEAS-2B cells was significantly higher than that in the H1299, A549, and H460 cells (Fig. 9D–E). To further determine the relationship between ADH1C and the generation of ROS in lung cancer cells, we knocked down ADH1C in H1299 and H460 cells (Fig. 9F). Subsequently, we detected significantly reduced enzymatic activities of HK, PK, LDH, and SDH in H1299 and H460 cells with knockdown of ADH1C (Fig. 9G), accompanied by much more ROS production (Fig. 9H). In addition, we used Mitotracker and TEM to detect mitochondrial damage in H1299 and H460 cells. We observed a significant increase in mitochondrial damage in cells after knocking down ADH1C (Fig. 9I–J), accompanied by an increase in TUNEL-positive cells in the cell population (Fig. 9K).

3.9. Correlation analysis of ADH1C and prognosis and immunotherapy in patients with lung cancer

Therefore, to further verify the relationship between ADH1C and the occurrence and development of lung cancer, we detected the expression level of ADH1C in 63 pairs of cancerous tissues and adjacent tissues. We found that the expression level and staining intensity of ADH1C in adjacent tissues were significantly lower than those in cancerous tissues (Fig. 10A–B). In previous results, we found that the expression level of ADH1C in lung cancer tissues was significantly higher than that in adjacent tissues. To further confirm the relationship between ADH1C and the prognosis of lung cancer patients, we further determined the correlation of ADH1C and the clinical phenotype of lung cancer patients. According to the analysis, patients with a relatively high expression level of ADH1C had a higher clinical TNM stage (Fig. 10C), and the tumor was less differentiated (Fig. 10D) but not related to tumor size or patient sex (Fig. 10E–F). Subsequently, we analyzed the survival time of patients based on the follow-up records, and the median expression level of ADH1C was used as the cut-off value to divide the patients into ADH1C high and low-expression groups. We observed that patients in the ADH1C low-expression group had a longer survival time (Fig. 10G). In addition, we also found that C1 cluster patients had a lower proportion of response to immunotherapy, so we further detected the expression levels of PD-L1 and HHLA2 in tumor tissues by qRT−PCR and analyzed the correlation between their expression levels and ADH1C by Spearman correlation analysis. We found that ADH1C was significantly and positively correlated with the expression of PD-L1 and HHLA2 (Fig. 10H).

4. Discussion

Lung cancer poses a great threat to humanity as a global disease. For those patients with advanced stages, immunotherapy seems to be a promising therapeutic option [19,20]. Despite the encouraging antitumour effects achieved by immune checkpoint inhibitors, many cancer patients do not respond or are less sensitive to these drugs, possibly through several mechanisms that inhibit antitumour immune effects in the unfavorable tumor microenvironment and metabolic conditions [21]. Metabolic changes in lung cancer can affect prognosis and response to treatment. Mitochondria are the energy factories of cells, and abnormalities in mitochondrial energy metabolic pathways are closely related to the development of lung cancer [22]. The energy metabolic pathways that tumor cells rely on for survival include glycolysis and mitochondrial oxidative phosphorylation [23]. Aberrant mitochondria-related pathways and metabolic disorders affecting gene expression contribute to cancer development and progression, as well as escape of the immune system [24]. Thus, abnormal energy production may be caused by mutations and altered expression of genes associated with the mitochondrial energy metabolic pathway (MEMP) [25]. Key genes involved in the mitochondrial energy metabolism system may affect the prognosis of lung adenocarcinoma and serve as suitable therapeutic targets [26]. Therefore, it would be more valuable to evaluate the role of all mitochondria-related genes in lung cancer prognosis and immunotherapy.

In this study, we collected 129 MMGs from the MSIGDB project and quantified the activity of mitochondrial metabolism. All NSCLC patients were divided into C1 and C2 clusters based on the 26 prognosis-related MMGs. The results indicated that the patients in the C2 cluster had a higher level of mitochondrial metabolism. Clinical correlation analysis showed that the C2 patients had a higher percentage of older patients, indicating different metabolism patterns in patients of different ages. Evidence from the TCGA and combined GEO cohorts indicated that patients in the C2 cluster responded better to immunotherapy and had a lower level of T-cell exclusion. Moreover, we found that all the markers of T-cell failure were upregulated in the C1 patients. The biological and immune microenvironment differences were then investigated between C1 and C2 patients.

Hypoxia is a prominent feature of the TME in solid tumors and is thought to be a major factor driving adaptation to host immune surveillance evasion [27]. Although the exact mechanism remains unclear, it is believed that hypoxic stress impedes immune cell function by inducing the expression and production of immunosuppressive molecules and metabolites in tumor cells [28]. In tumor cells, hypoxia triggers angiogenesis, epithelial mesenchymal transition (EMT) and metabolic reprogramming, as well as immune regulation [29–31]. T cell fate is closely linked to metabolic status. Cell activation occurs with the involvement of aerobic glycolysis and induces an increase in mitochondrial oxidative phosphorylation (OXPHOS) activity [32]. This leads to excessive ROS production, resulting in chronic inflammation, which is one of the environmental factors contributing to tumor immunosuppression [33]. Notably, we found that hypoxia can lead to a high percentage of C1 patients. Through further exploration of prognosis-related MMGs, we found that ADH1C might be involved in mitochondrial metabolism and immunotherapy response, which can be affected by hypoxia, making it an underlying biomarker.

When T cells are continuously stimulated by antigens, such as chronic infection and cancer, the cells cannot effectively develop and differentiate, and T cells become exhausted, which is called T-cell failure. In fact, T-cell failure is a key factor responsible for the immunosuppression status of the TME, as well as cancer immunotherapy [34]. Due to T-cell failure, many patients receiving immunotherapy, such as PD-1 or PD-L1 inhibitors, will not have a lasting antitumour response [35]. Consequently, immunotherapy can often be improved by reversing T-cell depletion, which has become a new research focus. Metabolic remodelling is a characteristic of exhausted T cells, especially mitochondrial metabolism [36]. In our study, 26 prognosis-related MMGs were identified and used for genotyping (C1 and C2 clusters). The patients in the C2 cluster had a higher mitochondrial metabolism level and a better prognosis. In lung cancer, Liu et al. demonstrated that S100A4 can enhance the malignant biological behaviors of lung cancer by upregulating the mitochondrial complex I protein NDUFS2 and affecting metabolism levels [37]. Xie et al. indicated that brusatol (a bioactive ingredient of traditional Chinese medicine) can affect NSCLC apoptosis by mediating the antioxidant response dependent on mitochondrial metabolism [38]. Moreover, we noticed that the C1 patients had a higher level of T-cell exclusion and corresponding markers. These results showed that the patients in the C1 and C2 clusters might have different mitochondrial metabolism patterns, which are responsible for the underlying biological differences.

We also noticed a higher genomic instability in C1 patients, such as TMB and MSI levels. Genomic instability is a hallmark of cancer [39]. Venkatesan et al. found that APOBEC3 can induce DNA replication stress and chromosomal instability in lung cancer and facilitate cancer progression [40]. Zhang et al. indicated that CDK7 can increase DNA replication stress and genomic instability and trigger immune response signals in NSCLC [41]. Meanwhile, GSEA indicated that pathways of G2M checkpoints, TNF-α signaling, E2F targets, EMT, MYC targets, and inflammatory response were significantly enriched in C1 patients. Hung et al. indicated that in NSCLC, bavachinin induces cancer cell G2/M arrest and apoptosis through ATM/ATR signaling [42]. Thompson et al. found that the gene signatures associated with EMT can accurately predict lung cancer responses to immune checkpoint blockade [43]. Yang et al. found that KRT6A can promote malignant biological behaviors in NSCLC in an EMT-dependent manner [44]. These results indicated that the above pathways might be responsible for the poor prognosis of patients in the C1 cluster.

Finally, we found that ADH1C might be involved in mitochondrial metabolism and the immunotherapy response, which can be affected by hypoxia. Offermans et al. indicated that ADH1C might be associated with alcohol intake and the occurrence of colon cancer [45]. In lung cancer, Feng et al. found that ADH1C can affect the cell cycle and promote cisplatin resistance [46]. According to our results in the preliminary raw letter analysis, ADH1C showed a significant negative correlation with TIDE in lung cancer patients. We found that the expression of ADH1C was significantly increased in people older than 65 years old, and ADH1C was significantly correlated with the activity of fatty acid metabolism, bile acid metabolism, and KRAS signaling pathways. In addition, ADH1C is upregulated in lung cancer cells and associated with ROS. We detected a significant reduction in the enzymatic activities of HK, PK, LDH and SDH in H1299 and H460 cells with knockdown of ADH1C, accompanied by more ROS. ADH1C was closely related to the prognosis of lung cancer patients, and we observed that patients in the ADH1C low-expression group had a longer survival time. Furthermore, we detected the expression levels of PD-L1 and HHLA2 in the tumor tissues and found that ADH1C was significantly and positively correlated with the expression of PD-L1 and HHLA2.

In summary, our study comprehensively explored whether ADH1C might be involved in mitochondrial metabolism and immunotherapy response, accompanied by ROS generation, making it an underlying biomarker of lung cancer.

Ethics statement

The cell lines used in this research were purchased from the Cell Resource Center of Peking Union Medical College (PCRC, Beijing, China). The Ethics Committee of Tongji Hospital, Tongji Medical College, Huazhong University of Science and Technology (Hubei, China) conducted a review and granted approval for the study. The number is TJ-IRB20210222.

Availability of data and material

The original contributions presented in the study are included in the article/supplementary material, and further inquiries can be directed to the corresponding author.

Funding statement

This work was supported by the State Key Program of National Natural Science of China (Grant No. 82130092) for Xianglin Yuan and the National Natural Science Foundation of China (grant number 82303355) for Zhe Tang.

CRediT authorship contribution statement

Sheng Wang: Writing – original draft, Visualization, Validation, Investigation, Formal analysis, Data curation. **Bo Liu:** Writing – review & editing, Supervision. **Fang Li:** Formal analysis, Data curation. **Zhe Tang:** Supervision, Resources, Funding acquisition. **Xuyu Gu:** Writing – review & editing, Supervision, Software, Project administration, Conceptualization. **Xianglin Yuan:** Supervision, Resources, Project administration, Funding acquisition, Conceptualization.

Declaration of competing interest

The authors declare that they have no known competing financial interests or personal relationships that could have appeared to influence the work reported in this paper.

Acknowledgements

We thank the analytical data provided by the TCGA and GEO databases.

Appendix A. Supplementary data

Supplementary data to this article can be found online at https://doi.org/10.1016/j.heliyon.2024.e27022.

References

[1] S. Thangudu, C.C. Yu, C.L. Lee, M.C. Liao, C.H. Su, Magnetic, biocompatible FeCO3 nanoparticles for T2-weighted magnetic resonance imaging of in vivo lung tumors, J. Nanobiotechnol. 20 (1) (2022 Mar 25) 157, https://doi.org/10.1186/s12951-022-01355-3. PMID: 35337331; PMCID: PMC8952886.
[2] N. Wang, C. Yu, T. Xu, D. Yao, L. Zhu, Z. Shen, X. Huang, Self-assembly of DNA nanostructure containing cell-specific aptamer as a precise drug delivery system for cancer therapy in non-small cell lung cancer, J. Nanobiotechnol. 20 (1) (2022 Nov 19) 486, https://doi.org/10.1186/s12951-022-01701-5. PMID: 36403038; PMCID: PMC9675138.
[3] X. Wang, T. Wang, J. Hua, M. Cai, Z. Qian, C. Wang, H. Li, S.E. McMillin, H.E. Aaron, C. Xie, H. Lin, Histological types of lung cancer attributable to fine particulate, smoking, and genetic susceptibility, Sci. Total Environ. 858 (Pt 2) (2023 Feb 1) 159890, https://doi.org/10.1016/j.scitotenv.2022.159890. Epub 2022 Nov 2. PMID: 36334679.
[4] X. Lin, R. Ye, Z. Li, B. Zhang, Y. Huang, J. Du, B. Wang, H. Meng, H. Xian, X. Yang, X. Zhang, Y. Zhong, Z. Huang, KIAA1429 promotes tumorigenesis and gefitinib resistance in lung adenocarcinoma by activating the JNK/MAPK pathway in an m6A-dependent manner, Drug Resist. Updates 66 (2023 Jan) 100908, https://doi.org/10.1016/j.drup.2022.100908. Epub 2022 Dec 5. PMID: 36493511.
[5] T. Wu, Y. Dai, Tumor microenvironment and therapeutic response, Cancer Lett. 387 (2017 Feb 28) 61–68, https://doi.org/10.1016/j.canlet.2016.01.043. Epub 2016 Feb 1. PMID: 26845449.
[6] A.R. Lim, W.K. Rathmell, J.C. Rathmell, The tumor microenvironment as a metabolic barrier to effector T cells and immunotherapy, Elife 9 (2020 May 5) e55185, https://doi.org/10.7554/eLife.55185. PMID: 32367803; PMCID: PMC7200151.
[7] K. Suresh, J. Naidoo, C.T. Lin, S. Danoff, Immune checkpoint immunotherapy for non-small cell lung cancer: benefits and pulmonary toxicities, Chest 154 (6) (2018 Dec) 1416–1423, https://doi.org/10.1016/j.chest.2018.08.1048. Epub 2018 Sep 4. PMID: 30189190; PMCID: PMC6335259.
[8] L. Liu, Y. Qu, L. Cheng, C.W. Yoon, P. He, A. Monther, T. Guo, S. Chittle, Y. Wang, Engineering chimeric antigen receptor T cells for solid tumour therapy, Clin. Transl. Med. 12 (12) (2022 Dec) e1141, https://doi.org/10.1002/ctm2.1141. PMID: 36495108; PMCID: PMC9736813.
[9] G.S.R. Raju, E. Pavitra, G.L. Varaprasad, S.S. Bandaru, G.P. Nagaraju, B. Farran, Y.S. Huh, Y.K. Han, Nanoparticles mediated tumor microenvironment modulation: current advances and applications, J. Nanobiotechnol. 20 (1) (2022 Jun 14) 274, https://doi.org/10.1186/s12951-022-01476-9. PMID: 35701781; PMCID: PMC9195263.
[10] D.B. Zorov, M. Juhaszova, S.J. Sollott, Mitochondrial reactive oxygen species (ROS) and ROS-induced ROS release, Physiol. Rev. 94 (3) (2014 Jul) 909–950, https://doi.org/10.1152/physrev.00026.2013. PMID: 24987008; PMCID: PMC4101632.
[11] E.M. Garrido-Martin, T.W.P. Mellows, J. Clarke, A.P. Ganesan, O. Wood, A. Cazaly, G. Seumois, S.J. Chee, A. Alzetani, E.V. King, C.C. Hedrick, G. Thomas, P. S. Friedmann, C.H. Ottensmeier, P. Vijayanand, T. Sanchez-Elsner, M1hot tumor-associated macrophages boost tissue-resident memory T cells infiltration and survival in human lung cancer, J Immunother Cancer 8 (2) (2020 Jul) e000778, https://doi.org/10.1136/jitc-2020-000778. PMID: 32699181; PMCID: PMC7375465.
[12] K. Pang, Z.D. Shi, L.Y. Wei, Y. Dong, Y.Y. Ma, W. Wang, G.Y. Wang, M.Y. Cao, J.J. Dong, Y.A. Chen, P. Zhang, L. Hao, H. Xu, D. Pan, Z.S. Chen, C.H. Han, Research progress of therapeutic effects and drug resistance of immunotherapy based on PD-1/PD-L1 blockade, Drug Resist. Updates 66 (2023 Jan) 100907, https://doi.org/10.1016/j.drup.2022.100907. Epub 2022 Nov 30. PMID: 36527888.
[13] J. Yu, M.D. Green, S. Li, Y. Sun, S.N. Journey, J.E. Choi, S.M. Rizvi, A. Qin, J.J. Waninger, X. Lang, Z. Chopra, I. El Naqa, J. Zhou, Y. Bian, L. Jiang, A. Tezel, J. Skvarce, R.K. Achar, M. Sitto, B.S. Rosen, F. Su, S.P. Narayanan, X. Cao, S. Wei, W. Szeliga, L. Vatan, C. Mayo, M.A. Morgan, C.A. Schonewolf, K. Cuneo, I. Kryczek, V.T. Ma, C.D. Lao, T.S. Lawrence, N. Ramnath, F. Wen, A.M. Chinnaiyan, M. Cieslik, A. Alva, W. Zou, Liver metastasis restrains immunotherapy efficacy via macrophage-mediated T cell elimination, Nat. Med. 27 (1) (2021 Jan) 152–164, https://doi.org/10.1038/s41591-020-1131-x. Epub 2021 Jan 4. PMID: 33398162; PMCID: PMC8095049.
[14] D.C. Fuhrmann, B. Brüne, Mitochondrial composition and function under the control of hypoxia, Redox Biol. 12 (2017 Aug) 208–215, https://doi.org/10.1016/j.redox.2017.02.012. Epub 2017 Feb 24. PMID: 28259101; PMCID: PMC5333533.
[15] S. Hänzelmann, R. Castelo, J. Guinney, GSVA: gene set variation analysis for microarray and RNA-seq data, BMC Bioinf. 14 (2013 Jan 16) 7, https://doi.org/10.1186/1471-2105-14-7. PMID: 23323831; PMCID: PMC3618321.
[16] R.K. Powers, A. Goodspeed, H. Pielke-Lombardo, A.C. Tan, J.C. Costello, GSEA-InContext: identifying novel and common patterns in expression experiments, Bioinformatics 34 (13) (2018 Jul 1) i555–i564, https://doi.org/10.1093/bioinformatics/bty271. PMID: 29950010; PMCID: PMC6022535.
[17] J. Fu, K. Li, W. Zhang, C. Wan, J. Zhang, P. Jiang, X.S. Liu, Large-scale public data reuse to model immunotherapy response and resistance, Genome Med. 12 (1) (2020 Feb 26) 21, https://doi.org/10.1186/s13073-020-0721-z. PMID: 32102694; PMCID: PMC7045518.
[18] B. Chen, M.S. Khodadoust, C.L. Liu, A.M. Newman, A.A. Alizadeh, Profiling tumor infiltrating immune cells with CIBERSORT, Methods Mol. Biol. 1711 (2018) 243–259, https://doi.org/10.1007/978-1-4939-7493-1_12. PMID: 29344893; PMCID: PMC5895181.

[19] X. Xiao, Y. Peng, Z. Wang, L. Zhang, T. Yang, Y. Sun, Y. Chen, W. Zhang, X. Chang, W. Huang, S. Tian, Z. Feng, N. Xinhua, Q. Tang, Y. Mao, A novel immune checkpoint siglec-15 antibody inhibits LUAD by modulating mφ polarization in TME, Pharmacol. Res. 181 (2022 Jul) 106269, https://doi.org/10.1016/j.phrs.2022.106269. Epub 2022 May 20. Erratum in: Pharmacol Res. 2022 Aug;182:106327. PMID: 35605813.

[20] Y. Hu, S. Paris, G. Bertolet, H.B. Barsoumian, K. He, D. Sezen, D. Chen, M. Wasley, J.D. Silva, J.A. Mitchell, T.A. Voss, F. Masrorpour, C.K. Leyton, L. Yang, C. Leuschner, N. Puebla-Osorio, S. Gandhi, Q.N. Nguyen, M.A. Cortez, J.W. Welsh, Combining a nanoparticle-mediated immunoradiotherapy with dual blockade of LAG3 and TIGIT improves the treatment efficacy in anti-PD1 resistant lung cancer, J. Nanobiotechnol. 20 (1) (2022 Sep 19) 417, https://doi.org/10.1186/s12951-022-01621-4. PMID: 36123677; PMCID: PMC9484155.

[21] A. Kalbasi, A. Ribas, Tumour-intrinsic resistance to immune checkpoint blockade, Nat. Rev. Immunol. 20 (1) (2020 Jan) 25–39, https://doi.org/10.1038/s41577-019-0218-4. Epub 2019 Sep 30. PMID: 31570880; PMCID: PMC8499690.

[22] B. Parma, H. Wurdak, P. Ceppi, Harnessing mitochondrial metabolism and drug resistance in non-small cell lung cancer and beyond by blocking heat-shock proteins, Drug Resist. Updates 65 (2022 Dec) 100888, https://doi.org/10.1016/j.drup.2022.100888. Epub 2022 Oct 28. PMID: 36332495.

[23] W.X. Zong, J.D. Rabinowitz, E. White, Mitochondria and cancer, Mol. Cell 61 (5) (2016 Mar 3) 667–676, https://doi.org/10.1016/j.molcel.2016.02.011. PMID: 26942671; PMCID: PMC4779192.

[24] K. Klein, K. He, A.I. Younes, H.B. Barsoumian, D. Chen, T. Ozgen, S. Mosaffa, R.R. Patel, M. Gu, J. Novaes, A. Narayanan, M.A. Cortez, J.W. Welsh, Role of mitochondria in cancer immune evasion and potential therapeutic approaches, Front. Immunol. 11 (2020 Oct 16) 573326, https://doi.org/10.3389/fimmu.2020.573326. PMID: 33178201; PMCID: PMC7596324.

[25] D.C. Wallace, Mitochondria and cancer, Nat. Rev. Cancer 12 (10) (2012 Oct) 685–698, https://doi.org/10.1038/nrc3365. PMID: 23001348; PMCID: PMC4371788.

[26] P. Ghosh, C. Vidal, S. Dey, L. Zhang, Mitochondria targeting as an effective strategy for cancer therapy, Int. J. Mol. Sci. 21 (9) (2020 May 9) 3363, https://doi.org/10.3390/ijms21093363. PMID: 32397535; PMCID: PMC7247703.

[27] Q. Wu, L. You, E. Nepovimova, Z. Heger, W. Wu, K. Kuca, V. Adam, Hypoxia-inducible factors: master regulators of hypoxic tumor immune escape, J. Hematol. Oncol. 15 (1) (2022 Jun 3) 77, https://doi.org/10.1186/s13045-022-01292-6. PMID: 35659268; PMCID: PMC9166526.

[28] F. Paredes, H.C. Williams, A. San Martin, Metabolic adaptation in hypoxia and cancer, Cancer Lett. 502 (2021 Apr 1) 133–142, https://doi.org/10.1016/j.canlet.2020.12.020. Epub 2021 Jan 11. PMID: 33444690; PMCID: PMC8158653.

[29] L. Schito, Hypoxia-dependent angiogenesis and lymphangiogenesis in cancer, Adv. Exp. Med. Biol. 1136 (2019) 71–85, https://doi.org/10.1007/978-3-030-12734-3_5. PMID: 31201717.

[30] S. Suthen, C.J. Lim, P.H.D. Nguyen, C.A. Dutertre, H.L.H. Lai, M. Wasser, C. Chua, T.K.H. Lim, W.Q. Leow, T.J. Loh, W.K. Wan, Y.H. Pang, G. Soon, P.C. Cheow, J.H. Kam, S. Iyer, A. Kow, W.L. Tam, T.W.H. Shuen, H.C. Toh, Y.Y. Dan, G.K. Bonney, C.Y. Chan, A. Chung, B.K.P. Goh, W. Zhai, F. Ginhoux, P.K.H. Chow, S. Albani, V. Chew, Hypoxia-driven immunosuppression by Treg and type-2 conventional dendritic cells in HCC, Hepatology 76 (5) (2022 Nov) 1329–1344, https://doi.org/10.1002/hep.32419. Epub 2022 Mar 17. PMID: 35184329.

[31] X. Zhang, B. Sai, F. Wang, L. Wang, Y. Wang, L. Zheng, G. Li, J. Tang, J. Xiang, Hypoxic BMSC-derived exosomal miRNAs promote metastasis of lung cancer cells via STAT3-induced EMT, Mol. Cancer 18 (1) (2019 Mar 13) 40, https://doi.org/10.1186/s12943-019-0959-5. PMID: 30866952; PMCID: PMC6417285.

[32] B. Banoth, S.L. Cassel, Mitochondria in innate immune signaling, Transl. Res. 202 (2018 Dec) 52–68, https://doi.org/10.1016/j.trsl.2018.07.014. Epub 2018 Aug 7. PMID: 30165038; PMCID: PMC6218307.

[33] K.B. Kennel, F.R. Greten, Immune cell - produced ROS and their impact on tumor growth and metastasis, Redox Biol. 42 (2021 Jun) 101891, https://doi.org/10.1016/j.redox.2021.101891. Epub 2021 Feb 5. PMID: 33583736; PMCID: PMC8113043.

[34] J. Crespo, H. Sun, T.H. Welling, Z. Tian, W. Zou, T cell anergy, exhaustion, senescence, and stemness in the tumor microenvironment, Curr. Opin. Immunol. 25 (2) (2013 Apr) 214–221, https://doi.org/10.1016/j.coi.2012.12.003. Epub 2013 Jan 6. PMID: 23298609; PMCID: PMC3636159.

[35] B. Wang, W. Zhang, V. Jankovic, J. Golubov, P. Poon, E.M. Oswald, C. Gurer, J. Wei, I. Ramos, Q. Wu, J. Waite, M. Ni, C. Adler, Y. Wei, L. Macdonald, T. Rowlands, S. Brydges, J. Siao, W. Poueymirou, D. MacDonald, G.D. Yancopoulos, M.A. Sleeman, A.J. Murphy, D. Skokos, Combination cancer immunotherapy targeting PD-1 and GITR can rescue CD8+ T cell dysfunction and maintain memory phenotype, Sci Immunol 3 (29) (2018 Nov 2) eaat7061, https://doi.org/10.1126/sciimmunol.aat7061. PMID: 30389797.

[36] A.L. Xia, J.C. Wang, K. Yang, D. Ji, Z.M. Huang, Y. Xu, Genomic and epigenomic perspectives of T-cell exhaustion in cancer, Brief Funct Genomics 18 (2) (2019 Mar 22) 113–118, https://doi.org/10.1093/bfgp/ely005. PMID: 29518177.

[37] L. Liu, L. Qi, T. Knifley, D.W. Piecoro, P. Rychahou, J. Liu, M.I. Mitov, J. Martin, C. Wang, J. Wu, H.L. Weiss, D.A. Butterfield, B.M. Evers, K.L. O'Connor, M. Chen, S100A4 alters metabolism and promotes invasion of lung cancer cells by up-regulating mitochondrial complex I protein NDUFS2, J. Biol. Chem. 294 (18) (2019 May 3) 7516–7527, https://doi.org/10.1074/jbc.RA118.004365. Epub 2019 Mar 18. PMID: 30885944; PMCID: PMC6509482.

[38] J. Xie, Z. Lai, X. Zheng, H. Liao, Y. Xian, Q. Li, J. Wu, S. Ip, Y. Xie, J. Chen, Z. Su, Z. Lin, X. Yang, Apoptotic activities of brusatol in human non-small cell lung cancer cells: involvement of ROS-mediated mitochondrial-dependent pathway and inhibition of Nrf2-mediated antioxidant response, Toxicology 451 (2021 Mar 15) 152680, https://doi.org/10.1016/j.tox.2021.152680. Epub 2021 Jan 16. PMID: 33465425.

[39] D. Hanahan, R.A. Weinberg, Hallmarks of cancer: the next generation, Cell 144 (5) (2011 Mar 4) 646–674, https://doi.org/10.1016/j.cell.2011.02.013. PMID: 21376230.

[40] S. Venkatesan, M. Angelova, C. Puttick, H. Zhai, D.R. Caswell, W.T. Lu, M. Dietzen, P. Galanos, K. Evangelou, R. Bellelli, E.L. Lim, T.B.K. Watkins, A. Rowan, V. H. Teixeira, Y. Zhao, H. Chen, B. Ngo, L.P. Zalmas, M. Al Bakir, S. Hobor, E. Grönroos, A. Pennycuick, E. Nigro, B.B. Campbell, W.L. Brown, A.U. Akarca, T. Marafioti, M.Y. Wu, M. Howell, S.J. Boulton, C. Bertoli, T.R. Fenton, R.A.M. de Bruin, A. Maya-Mendoza, E. Santoni-Rugiu, R.E. Hynds, V.G. Gorgoulis, M. Jamal-Hanjani, N. McGranahan, R.S. Harris, S.M. Janes, J. Bartkova, S.F. Bakhoum, J. Bartek, N. Kanu, C. Swanton, TRACERx Consortium, Induction of APOBEC3 exacerbates DNA replication stress and chromosomal instability in early breast and lung cancer evolution, Cancer Discov. 11 (10) (2021 Oct) 2456–2473, https://doi.org/10.1158/2159-8290.CD-20-0725. Epub 2021 May 4. PMID: 33947663; PMCID: PMC8487921.

[41] H. Zhang, C.L. Christensen, R. Dries, M.G. Oser, J. Deng, B. Diskin, F. Li, Y. Pan, X. Zhang, Y. Yin, E. Papadopoulos, Y. Pyon, C. Thakurdin, N. Kwiatkowski, K. Jani, A.R. Rabin, D.M. Castro, T. Chen, H. Silver, Q. Huang, M. Bulatovic, C.M. Dowling, B. Sundberg, A. Leggett, M. Ranieri, H. Han, S. Li, A. Yang, K. E. Labbe, C. Almonte, V.O. Sviderskiy, M. Quinn, J. Donaghue, E.S. Wang, T. Zhang, Z. He, V. Velcheti, P.S. Hammerman, G.J. Freeman, R. Bonneau, W. G. Kaelin Jr., K.D. Sutherland, A. Kersbergen, A.J. Aguirre, G.C. Yuan, E. Rothenberg, G. Miller, N.S. Gray, K.K. Wong, CDK7 inhibition potentiates Genome instability triggering anti-tumor immunity in small cell lung cancer, Cancer Cell 37 (1) (2020 Jan 13) 37–54.e9, https://doi.org/10.1016/j.ccell.2019.11.003. Epub 2019 Dec 26. PMID: 31883968; PMCID: PMC7277075.

[42] S.Y. Hung, S.C. Lin, S. Wang, T.J. Chang, Y.T. Tung, C.C. Lin, C.T. Ho, S. Li, Bavachinin induces G2/M cell cycle arrest and apoptosis via the ATM/ATR signaling pathway in human small cell lung cancer and shows an antitumor effect in the xenograft model, J. Agric. Food Chem. 69 (22) (2021 Jun 9) 6260–6270, https://doi.org/10.1021/acs.jafc.1c01657. Epub 2021 May 27. PMID: 34043345.

[43] J.C. Thompson, W.T. Hwang, C. Davis, C. Deshpande, S. Jeffries, Y. Rajpurohit, V. Krishna, D. Smirnov, R. Verona, M.V. Lorenzi, C.J. Langer, S.M. Albelda, Gene signatures of tumor inflammation and epithelial-to-mesenchymal transition (EMT) predict responses to immune checkpoint blockade in lung cancer with high accuracy, Lung Cancer 139 (2020 Jan) 1–8, https://doi.org/10.1016/j.lungcan.2019.10.012. Epub 2019 Oct 18. PMID: 31683225; PMCID: PMC7176049.

[44] B. Yang, W. Zhang, M. Zhang, X. Wang, S. Peng, R. Zhang, KRT6A promotes EMT and cancer stem cell transformation in lung adenocarcinoma, Technol. Cancer Res. Treat. 19 (2020 Jan-Dec) 1533033820921248, https://doi.org/10.1177/1533033820921248. PMID: 32329414; PMCID: PMC7225834.

[45] N.S.M. Offermans, S.M. Ketcham, P.A. van den Brandt, M.P. Weijenberg, C.C.J.M. Simons, Alcohol intake, ADH1B and ADH1C genotypes, and the risk of colorectal cancer by sex and subsite in The Netherlands Cohort Study, Carcinogenesis 39 (3) (2018 Mar 8) 375–388, https://doi.org/10.1093/carcin/bgy011. PMID: 29390059.

[46] F. Jiang, Q. Shen, F. Zhang, J. Fu, L. Hu, J. Wang, H. Zhou, J. Chen, Y. Wang, ADH1C facilitates cisplatin resistance of lung adenocarcinoma cells, DNA Cell Biol. 41 (6) (2022 Jun) 631–640, https://doi.org/10.1089/dna.2021.0877. Epub 2022 May 24. PMID: 35612423.